APPLICATION OF A MAGNETIC SUSPENSION BALANCE TO THE OXIDATION STUDY OF THE ZIRCONIUM BASED ALLOYS UNDER HIGH PRESSURE WATER VAPOUR

Y. Dali[1], M. Tupin[1], P. Bossis[1], F. Valdivieso[2] and M. Pijolat[2]*

[1]CEA Saclay, DEN/DANS/DMN/SEMI/LM2E, 91191 Gif sur Yvette Cedex, France
[2]Ecole Nationale Supérieure des Mines, LPMG, URA CNRS 2021, Centre SPIN, 158 Cours Fauriel, 42023 Saint-Etienne, Cedex 2, France

The fuel claddings in the Pressurised Water Reactor are corroded in water at high temperature and high pressure. The technical device ableto follow continuously the corrosion rate in conditions close to this medium does not yet exist. That is the reason why a high pressure thermogravimetric installation based on magnetic suspension has been designed to study in situ the oxidation kinetics of the zirconium based alloys under water vapour until 50 bars of pressure at 415°C. The accuracy of measurements is about $5 \cdot 10^{-5}$ g under 2 bars, and 10^{-4} g under 50 bars. The reproducibility of measurements was verified and the deviation regarding post test weighing at room temperature is around $5 \cdot 10^{-5}$ g what is clearly satisfying. Finally, the results presented in this work allow validating the high pressure thermogravimetric measurements obtained with this magnetic suspension device.

Keywords: high pressure, kinetics, magnetic suspension, oxidation, steam, thermogravimetry, Zircaloy-4

Introduction

Zirconium based alloys are widely used as cladding material for fuel rods of water-cooled nuclear reactors because of their low neutron capture cross-section, good corrosion resistance in operating conditions and satisfying mechanical properties. The first family of zirconium based alloys is the Zircaloys, starting with Zircaloy-1, a sponge zirconium containing 1.5 mass% Sn. Tin was added to eliminate the negative effect of nitrogen. This element increases the strength but reduces the corrosion resistance [1]. A hazardous pollution of a Zircaloy-1 with an austenitic stainless steel (18% Cr and 8% Ni) led to the alloy called Zircaloy-2 which contains 1.2–1.7 mass% of Sn, 0.07–0.2 mass% Fe, 0.05–0.15 mass% Cr, 0.09–0.16 mass% O and 0.03–0.08 mass% Ni. Chromium and iron improve the corrosion resistance in water and steam, and the nickel improves the corrosion resistance in steam [2]. The last alloy developed is the Zircaloy-4 which does not contain any nickel because of its detrimental role in the hydrogen absorption [3].

Numerous studies in the last decades were performed to develop these alloys and to elucidate their particular corrosion kinetic behaviours [4]. For the first kinetic regime called the pre-transition, it is generally assumed that the growth of the oxide during this stage is controlled by the diffusion of the oxygen through the oxide. The mass gain curve in this case corresponds to a sub-parabolic law [5]. After this period, an acceleration of the mass gain results in the change in the oxide morphology. This phenomenon is called kinetic transition. Finally the mass gain law tends to become linear.

The oxidation mechanism of Zircaloy-4 is not yet well understood. For a long time, studying the corrosion process of zirconium alloy in high temperature and high pressure conditions has been done by discontinuous measurements of the mass gain. To improve the understanding of this corrosion process it is of great interest to perform at high pressure steam in situ measurements. Recently, we designed and built a new experimental device, based on a Rubotherm magnetic suspension balance, that allows to access continuously to the mass gain during the oxidation of zirconium based alloys in pure water vapour under high pressure. In this paper, experimental installation will be presented in first place and its principle will be detailed. Secondly, the qualifications tests will be described and analyzed.

Previously, some classical thermogravimetric microbalance tests on zirconium alloys were carried out but only at low partial pressure [6, 7]. For high pressure, the corrosion experiments performed in autoclaves consist of discontinuous mass gain measurements at different oxidation time. The only way to follow in situ the mass gain in these extreme conditions is to separate the balance and the measurement cell, from the corrosive medium and to couple magnetically the balance to the sample as proposed by Gast in 1959 [8, 9].

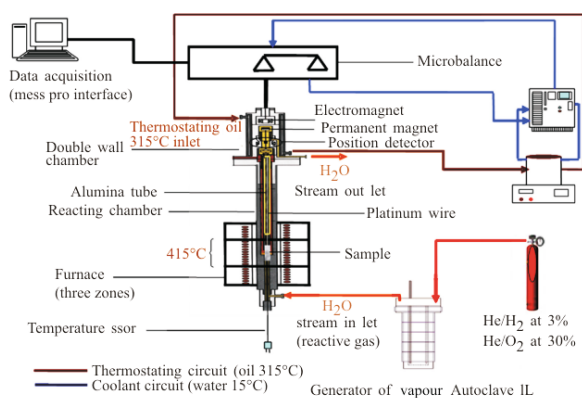* Author for correspondence: mpijolat@emse.fr

Fig. 1 General scheme of the experimental device

Experimental

As described in Fig. 1 the high pressure water vapour device is made up of different parts:

Steam generator

The steam generator consists of a one-liter autoclave connected to different atmospheres, inert gas (helium or argon), mixed helium-oxygen at 20% and diluted hydrogen at 3% in helium. The temperature, the hydrogen partial pressure and the whole pressure are controlled by thermocouples and pressure sensors. With this autoclave 150 bars of pure water vapour can be generated (maximal pressure of the Magnetic Suspension Balance (MSB)).

Heating system

The oxidation experiments are done around 400–450°C under high pressure steam. A three-zone furnace guarantees an isothermal zone of about 12 cm, covering the entire surface of tested samples (2·10 cm). Heating collars surrounding the different connecting tubes (reaching 400°C) allow to avoid condensation. They are regulated to be always over the water liquid-vapour equilibrium temperature.

Magnetic suspension balance

Developed by RUBOTHERM and based on a magnetic coupling system, the magnetic suspension balance is composed of:

- the microbalance (accuracy of 10^{-5} g);
- the electromagnet;
- the magnetic suspension composed of a permanent magnet, a sensor core and a coupling cone;
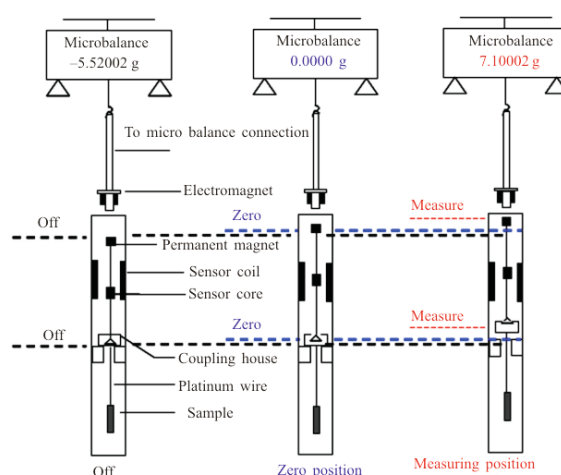- the coupling house at which the sample is hung via a platinum wire.

Fig. 2 Principle of the mass gain measurements by the magnetic suspension balance

The electromagnet is suspended to the microbalance, and maintains in levitation the magnetic suspension. As shown on Fig. 2, three positions are used to perform the mass gain measurements:

- OFF position: the magnetic suspension is not attracted by the electromagnet and so lays down on the coupling house;
- Zero position (ZP): there is no coupling between the magnetic suspension and the sample, this position corresponds to the tare;
- Measure position (MP): the sample is coupled to the magnetic suspension; the mass of the sample is deduced from the current flowing in the electromagnet (and measured in this position by the microbalance).

The succession of the two positions (ZP–MP) leads to in situ acquirement of the mass gain.

Thermostating circuit

As described in the Fig. 1, two thermostating circuits are used in this experiment. In the first one, a special high temperature oil flows inside the double wall chamber that allows to maintain the temperature up to 315°C in this part of the device and thus to avoid the water condensation. The second circuit is a cooling one; liquid water at 15°C flows inside a cooler diaphragm placed underneath the microbalance limiting the temperature in the microbalance. The circulation of the cold water is performed by a cryothermostat.

Pressure and temperature sensors

A two points temperature sensor is localised underneath the sample. These thermocouples allow the acquisition of two temperatures near the sample (the points are 5 cm apart). The temperature of the double wall chamber is controlled by an external thermocouple.

Two pressure sensors – connected to the autoclave cell – allow measuring the variation of the hydrogen pressure and of the total pressure (water vapour, inert gas and hydrogen).

Connecting tubes and valves

All the connections and valves are in a stainless steel tube adapted to high temperature and high pressure conditions, the introduction of gases in the tube-reactor is regulated by a high temperature and high pressure long valve (AT231).

Data acquisition

The Mess pro software allows to operate manually and also to perform measurement by programming different time segments (the maximum acquisition time is 2 months). All the electronic components are connected to the microbalance at ambient conditions.

Qualification tests

Specific tests have been performed to validate the experimental measurements, in particular signal accuracy, and to estimate the temperature stability, the buoyancy effect, the signal reproducibility and the effect of natural convection. The qualification tests were conducted on a Zircaloy-4 experimental alloy (sheet of 0.5 mm thickness) provided by AREVA NP CEZUS. Its composition is given in Table 1.

Signal accuracy

To validate the mass gain values measured by the thermobalance (magnetic suspension balance), three corrosion experiments at 415°C and different pressures have been performed on Zy4. These values of mass gains have been compared to mass variations of the samples measured after and before the corrosion with a classical balance (Sartorius) working at room temperature.

The mass gain values obtained with the two techniques and their discrepancy are given in Table 2.

Table 1 Chemical composition of the studied alloy

Alloy	Sn/	Cr/	Fe/	O/	Zr/
	mass%				
Zircaloy-4	1.46	0.107	0.22	0.126	Bal

It should be noticed that about 2 g difference in mass between the ordinary balance and the thermo-balance comes from the fact that the mass measured by the microbalance takes into account the mass of the sample but in addition the mass of the hook and the coupling house. From Table 2, the mass gain determined by the ordinary balance is in good agreement with the mass variation measured with the thermobalance. In consequence, the signal accuracy of our experimental device is validated up to 50 bars.

Stability of temperature

Our experiments are generally done under isothermal conditions over a long time period. That is the reason why different tests were done to verify the thermal stability inside the tube-reactor with a thermocouple located 1 cm underneath the sample. The temperature variations during 10 days of experiment for different temperature plateaus are shown in Fig. 3. The temperature fluctuations do not exceed ±2 °C during the isothermal plateau, and temperature stability is consequently relatively satisfying.

Buoyancy effect

Doing experiments under high pressures needs a quantification of the buoyancy effect. Indeed, by increasing the pressure, the density of the reactive gas changes leading to an apparent decrease in the mass gain as observed in Fig. 4 for five pressure plateaus at respectively 19, 30, 50, 80 and 100 bars, at 415°C.

The apparent mass loss resulting from the buoyancy effect can be theoretically calculated and then compared to the experimental results. Table 3 and Fig. 5 sum up the experimental mass loss and the calculated one considering the Archimedes' principle. The apparent mass change during a pressure change

Table 2 Mass gains obtained with balance at room temperature ('ordinary' balance) and with thermobalance for experiments at different pressures

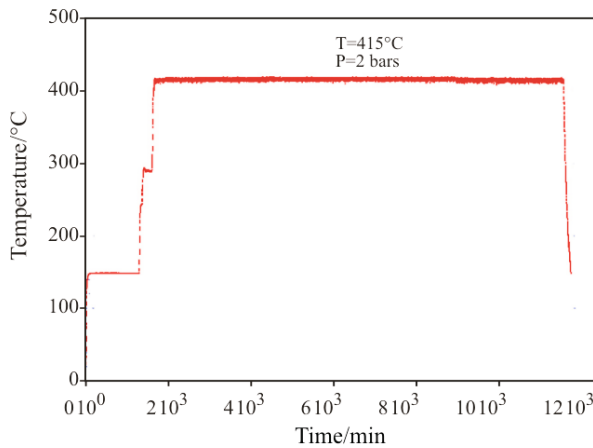|	'Ordinary' balance			Thermobalance			Mass difference
P/bar	initial mass/g	final mass/g	Δm_1/g	initial mass/g	final mass/g	Δm_2/g	Δm_2-Δm_1/g
2	8.10108	8.11145	0.01037	10.21394	10.22435	0.01041	0.00004
10	8.13409	8.14889	0.0148	10.23718	10.25195	0.01477	−0.00003
50	7.87105	7.88219	0.01114	9.9504	9.96155	0.01115	0.00001

Fig. 3 Temperature evolution for different isothermal plateaus (P_{H_2O}=2 bar)
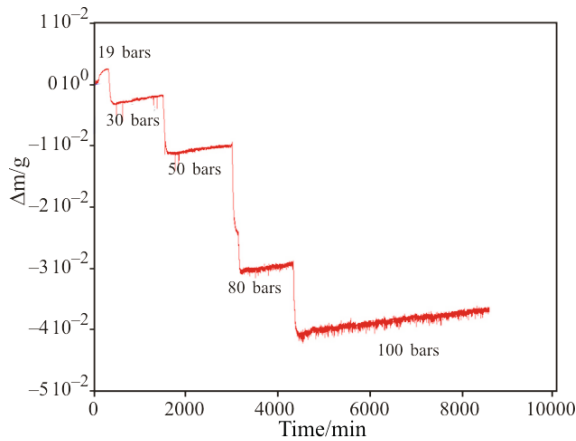

Fig. 4 Effect of pressure changes on the mass signal

Table 3 Values of mass loss, theoretically calculated and experimentally measured

Pressure increase/bar	Calc. mass loss due to the buoyancy/g	Mass loss given by the experimental results/g
19–30	$4.2 \cdot 10^{-3}$	$5.5 \cdot 10^{-3}$
30–50	$8.9 \cdot 10^{-3}$	$9.0 \cdot 10^{-3}$
50–80	$14.8 \cdot 10^{-3}$	$20 \cdot 10^{-3}$
80–100	$11.3 \cdot 10^{-3}$	$11 \cdot 10^{-3}$

from P_1 to P_2 due to buoyancy was calculated by the following formula (1):

$$\left| \Delta m \right| = V \times \left| \rho(P_2,T) - \rho(P_1,T) \right| \qquad (1)$$

where Δm is the mass variation during the pressure drop (mg), V the volume of the object (cm^3), and $\rho(P_1,T)$ and $\rho(P_2,T)$, the densities of the steam, respectively at the pressures P_1 and P_2 and the temperature T (mg cm^{-3}).

For instance, for the pressure change from 30 to 50 bars, we have to take into account the buoyancy effect on the masses of the sensor coil, the coupling house and the sample. But all these components are
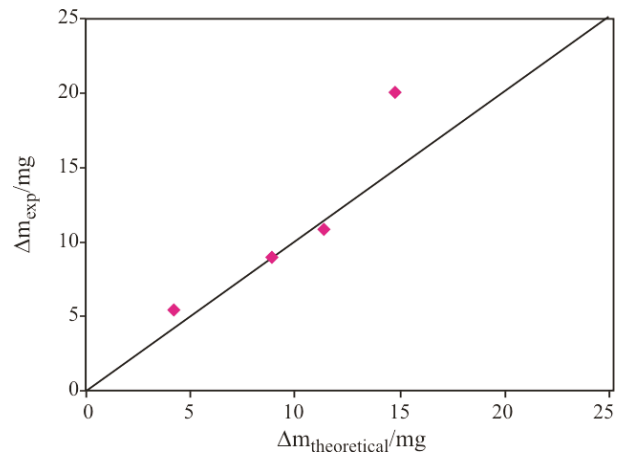

Fig. 5 Comparison between the calculated and the experimental mass loss due to the pressure change

not submitted to the same temperature, the sensor coil and the coupling house are actually at 320°C while the sample is corroded at 415°C. Consequently, the mass variations per volume unit are not the same because the steam densities are different at these temperatures. For this pressure drop, the mass loss can be detailed for each component:

- sensor coil:

$$\left| \Delta m \right| = V \times \left| \rho(50b,320°C) - \rho(30b,320°C) \right| =$$
$$= 0.82 \times (20.8 - 10.8) = 8.2 \text{ mg} \quad \text{with } V = 0.82 \text{ cm}^3$$

- coupling house:

$$\left| \Delta m \right| = V \times \left| \rho(50b,320°C) - \rho(30b,320°C) \right| =$$
$$= 0.23 \times (20.8 - 10.8) = 2.3 \text{ mg} \quad \text{with } V = 0.23 \text{ cm}^3$$

- sample:

$$\left| \Delta m \right| = V \times \left| \rho(50b,415°C) - \rho(30b,415°C) \right| =$$
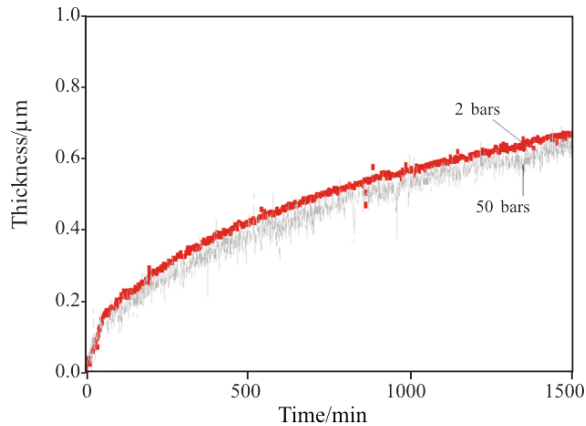$$= 0.85 \times (16.8 - 9) = 6.6 \text{ mg} \quad \text{with } V = 0.85 \text{ cm}^3$$

The superheated water densities come from [10].

The masses measured during the ZP measurement step and the MP one describe respectively the mass loss of the sensor coil and those of the three preceding elements. The mass variations indicated on the Fig. 5 correspond to the difference between the ZP measurement and the MP one. Thus the mass loss due to the buoyancy observed during the pressure drop results only from those calculated on the coupling house and the sample. It is equal to 8.9 mg and is so very close to the experimental value (Table 5).

As shown on Fig. 5, except for the surrounded point with approximately 20 mg, theoretical calculations are in relatively good agreement with the experimental results. It is so possible to correct the mass signal from the buoyancy effect during any experiment that includes temperature or pressure modification.

Table 4 Calculated Rayleigh numbers under different conditions (with ΔT=100°C)

T=573°C		T=673°C		T=773°C	
P/bar	Ra	P/bar	Ra	P/bar	Ra
10	$6\cdot10^7$	10	$5\cdot10^7$	10	$3\cdot10^7$
50	$3\cdot10^9$	50	$1\cdot10^9$	50	$8\cdot10^8$
100	$1\cdot10^{10}$	100	$7\cdot10^9$	100	$4\cdot10^9$

Fig. 6 Reproducibility of the thickness deduced from the mass
signal obtained with the thermobalance during
Zircaloy-4 oxidation at 415°C and 2 bars

Reproducibility test

As illustrated in Fig. 6, the measurements for two
experiments performed in the same conditions (415°C
and 2 bars) are clearly reproducible. The oxide thickness
is deduced from the mass gain by the following
formula (2):

$$X = \frac{1}{S_0} \frac{M_{ZrO_2}}{\rho_{ZrO_2}} \frac{\Delta m}{M_{O_2}} \qquad (2)$$

where ρ_{ZrO_2} is the mass density of zirconia (5.6 g cm^{-3}
for the monoclinic phase), M_{ZrO_2} and M_{O_2} are
respectively the molar masses of zirconia and oxygen
(g mol^{-1}), S_0 is the sample reacting surface (cm^2).
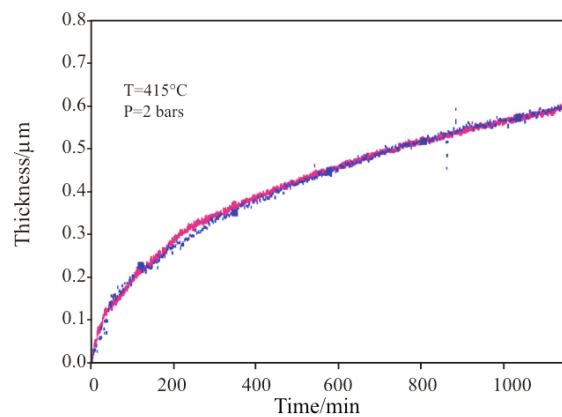
Natural convection

Natural convection phenomena are often frequent and
observed during thermogravimetric measurements
because of gas density variations inside the experimental
system, related to cold points and more generally to
temperature differences between two parts of the device.
The Rayleigh adimensional number allows to estimate
qualitatively the convection phenomena in a given
experimental system. It is defined as follows:

$$Ra = \frac{g\beta C_p \rho^2 b^3 \Delta T}{\eta K}$$

with g: acceleration of gravity (m s^{-2}), β: thermal
expansion coefficient (K^{-1}), C_p: heat-storage capacity
(J kg^{-1} K^{-1}), ρ: density (kg m^{-3}), b: length of the non-
isothermal zone (m), ΔT: temperature difference (K),
η: dynamic viscosity of gas (Pa s), K: thermal con-
ductivity of gas (W m^{-1} K^{-1}).

According to the literature [10], the threshold
value of the Rayleigh number, beyond which the
natural convection must be taken into account in this
kind of reactors, is about 40000. Rayleigh number
values were calculated for three different temperatures,
300, 400 and 500°C, and three different pressures 10,
50 and 100 bars applied to the sample, considering
that the temperature difference (DT) between the
magnetic suspension and the sample is in general
around 100°C. The results of these calculations are
presented in Table 4.

The Rayleigh number increases with increasing
pressure and the obtained values are always above the
threshold which means theoretically that convection
should take place in our tube-reactor. Whatever, when
the pressure is above 30 bars, in practice, the convection
currents disturb significantly the mass signal. For in-
stance, as shown on Fig. 7, the thickness variation *vs.*
time for an isobaric experiment at 50 bars is relatively
noisy compared to the one at 2 bars. For this pressure
range, it is thus important to limit these convection
currents as well as possible. In order to reduce the nat-
ural convection phenomena, the aim is to break the
currents of convection flowing inside the reacting
chamber, with a protection cage around the sample,
by creating obstacles such as an alumina tube.

Fig. 7 Oxide thickness variations of Zircaloy-4 oxidized at
415°C under 2 bars and 50 bars of water vapour

Conclusions

A high pressure thermogravimetric installation was developed allowing to study in situ the oxidation kinetics of the zirconium based alloys under pure water vapour until 50 bars of pressure at 415°C. Accuracy of measurements is about $5 \cdot 10^{-5}$ g under 2 bars, and 10^{-4} g under 50 bars. The reproducibility of measurements was verified and the deviation regarding post test weighing measurements at room temperature is about $5 \cdot 10^{-5}$ g.

Acknowledgements

References

1 B. G. Parfenov, V. V. Gerasimov and G. I. Venediktova, Corrosion of zirconium and zirconium alloys in Myers, New York 1967, p. 9.
2 B. Cox, J. Nucl. Mater., 336 (2005) 331.
3 E. Hillner, Hydrogen absorption in Zircaloy during aqueous corrosion, Effect of Environment, U.S. Rep. WAPD-TM-411, Bettis Atomic Power Lab, Pittsburgh 1964.
4 International Atomic Energy Agency, Waterside Corrosion of Zirconium in Nuclear Power Plants, IAEA-TECDOC-996, IAEA, Vienna 1998, p. 37.
5 P. Kofstad, High temperature corrosion in Elsevier Publishing, London–NewYork 1988, p. 299.
6 M. Tupin, M. Pijolat, F. Valdivieso, M. Soustelle, A. Frichet and P. Barberis, J. Nucl. Mater., 317 (2003) 130.
7 N. Pétigny-Putigny, Comparaison de l'oxydation de deux alliages à base de zirconium par diffraction des rayons X in-situ et ex-situ: texture, phase, contrainte, PhD thesis, Université de Bourgogne, Bourgogne 1998.
8 Th. Gast and W. Pahlke, J. Thermal Anal., 37 (1991) 1933.
9 Th. Gast and E. Robens, J. Thermal Anal., 47 (1996) 605.
10 C. A. Meyer, ASME Steam Tables in American Society of Mechanical Engineers, New York, 1983.
11 P. Sarrazin, A. Galerie and J. Foultier, Les mécanismes de corrosion sèche une approche cinétique in EDP Science, Paris, 2000, p. 44.